T cell Activation Is Driven by an ADP-Dependent Glucokinase Linking Enhanced Glycolysis with Mitochondrial Reactive Oxygen Species Generation

Marcin M. Kamiński,[1,7,*] Sven W. Sauer,[4,7] Marian Kamiński,[5] Silvana Opp,[4] Thorsten Ruppert,[4] Paulius Grigaravičius,[2] Przemysław Grudnik,[6] Hermann-Josef Gröne,[3] Peter H. Krammer,[1] and Karsten Gülow[1,*]

[1]Division of Immunogenetics (D030), Tumour Immunology Program
[2]Junior Research Group DNA Repair and CNS Diseases (G390)
[3]Department of Cellular and Molecular Pathology (G130)
German Cancer Research Center (DKFZ), 69120 Heidelberg, Germany
[4]Department of General Pediatrics, Division of Inborn Metabolic Diseases, University Children's Hospital, 69120 Heidelberg, Germany
[5]Department of Chemical and Process Engineering, Chemical Faculty, Gdańsk University of Technology, 80-233 Gdańsk, Poland
[6]Department of Microbiology, Faculty of Biochemistry, Biophysics and Biotechnology, Jagiellonian University, 31-007 Kraków, Poland
[7]These authors contributed equally to this work
*Correspondence: m.kaminski@dkfz.de (M.M.K.), k.guelow@dkfz.de (K.G.)
http://dx.doi.org/10.1016/j.celrep.2012.10.009

SUMMARY

Mitochondria-originating reactive oxygen species (ROS) control T cell receptor (TCR)-induced gene expression. Here, we show that TCR-triggered activation of ADP-dependent glucokinase (ADPGK), an alternative, glycolytic enzyme typical for *Archaea*, mediates generation of the oxidative signal. We also show that ADPGK is localized in the endoplasmic reticulum and suggest that its active site protrudes toward the cytosol. The ADPGK-driven increase in glycolytic metabolism coincides with TCR-induced glucose uptake, downregulation of mitochondrial respiration, and deviation of glycolysis toward mitochondrial glycerol-3-phosphate dehydrogenase (GPD) shuttle; i.e., a metabolic shift to aerobic glycolysis similar to the Warburg effect. The activation of respiratory-chain-associated GPD2 results in hyperreduction of ubiquinone and ROS release from mitochondria. In parallel, mitochondrial bioenergetics and ultrastructure are altered. Downregulation of ADPGK or GPD2 abundance inhibits oxidative signal generation and induction of NF-κB-dependent gene expression, whereas overexpression of ADPGK potentiates them.

INTRODUCTION

Stimulation of the T cell receptor (TCR) drives T cells into rapid proliferation and differentiation. After PLCγ1 induction, the TCR response splits into two pathways. Inositol 3,4,5-triphosphate induces a rise in cytosolic Ca^{2+} and activation of Ca^{2+}-dependent transcription factors, e.g., nuclear factor of activated T cells (NF-AT). Diacylglycerol (DAG) activates protein kinase Cθ

(PKCθ) and RAS guanyl nucleotide-releasing protein (RasGRP), leading to triggering of NF-κB and AP-1. These three transcription factors essentially control activation-induced gene expression. Thus, simultaneous treatment with a Ca^{2+} ionophore, e.g., ionomycin (Iono), and a DAG mimetic, phorbol 12-myristate 13-acetate (PMA), yields T cell activation-driven transcriptional response. T cell activation is paralleled by transient generation of low, physiologically relevant levels of reactive oxygen species (ROS), i.e., an H_2O_2-mediated oxidative signal, which facilitates activation of ROS-dependent transcription factors, NF-κB and AP-1 (Dröge, 2002; Kamiński et al., 2010, 2012). This oxidative signal is indispensible for T cell activation (Devadas et al., 2002; Dröge, 2002; Kamiński et al., 2010). Together with a Ca^{2+} influx, it constitutes the minimal requirement for activation-induced gene expression (e.g., interleukin 2 [IL-2], IL-4, CD95 ligand [L]) (Devadas et al., 2002; Gülow et al., 2005; Kamiński et al., 2007, 2010). Different enzymatic sources, such as the respiratory chain (Kamiński et al., 2007, 2010, 2012; Yi et al., 2006), lipoxygenases (Los et al., 1995), and NADPH oxidases (NOX2, DUOX2) (Jackson et al., 2004; Kwon et al., 2010), have been described as participating in T cell activation-triggered ROS production. Our previous work demonstrates a crucial role for mitochondria as the source of the oxidative signal. We showed that TCR-induced PKCθ activation drives complex-I-mediated mitochondrial ROS production. $O_2^{-\cdot}$ released into the mitochondrial matrix is converted into H_2O_2 by superoxide dismutase (MnSOD, SOD2) (Kamiński et al., 2007, 2012). H_2O_2 diffuses into the cytoplasm to act as an oxidative signal mediator. MnSOD, upregulated during the late phase of a TCR-induced response, is considered a critical regulator of oxidative signal generation (Kamiński et al., 2012).

The intracellular redox equilibrium is controlled by a network of enzymatic and nonenzymatic factors that partially substitute for each other, as in the case of alternative enzymatic sources of the TCR-induced oxidative signal. In addition, TCR-triggered gene expression is also controlled by redox-independent transcription factors, e.g., NF-AT, SP-1, Oct-1, or CREB. Nevertheless, direct

block of ROS release from mitochondria by complex I inhibitors, small interfering RNA (siRNA)-mediated downregulation of NDUFAF1 (an assembly factor for complex I), or upregulation of MnSOD above its threshold level efficiently inhibit T cell activation-induced gene expression (Kamiński et al., 2007, 2012). Thus, mitochondria-derived ROS are essential for gene expression upon TCR stimulation.

T cell activation-induced gene expression depends on glucose uptake (Jacobs et al., 2008; Stentz and Kitabchi, 2005) and is accompanied by a metabolic switch from mitochondrial ATP production to aerobic glycolysis, i.e., the Warburg effect (Wang et al., 1976; Warburg, 1956), a phenomenon also characteristic for fast-proliferating cancer cells (Vander Heiden et al., 2009; Warburg, 1956). Cancer cells are often endowed with high intrinsic ROS production and constitutive NF-κB activation (Baud and Karin, 2009; Wellen and Thompson, 2010). Upregulated glucose metabolism under hyperglycemic and hypoxic conditions was also shown to induce mitochondrial ROS release in different cellular systems (Bell et al., 2007; Nishikawa et al., 2000; Wellen and Thompson, 2010). Thus, it is possible that upon T cell activation, the mitochondrial respiratory chain switches from an ATP-producing to an oxidative signaling function while glycolysis responds to cellular energy demands. Therefore, we studied metabolic changes accompanying generation of the oxidative signal (i.e., occurring within 1 hr of TCR or PMA triggering) (Kamiński et al., 2007, 2012) in partially glycolytic, proliferating cells—in vitro expanded peripheral human T cells (Bental and Deutsch, 1993) and Jurkat T cells (Miccheli et al., 2006).

RESULTS

TCR Triggering Induces a Metabolic Shift in T Cells

Reduction of mitochondrial respiration and increase in glycolysis are central to the Warburg effect (Vander Heiden et al., 2009; Wang et al., 1976; Warburg, 1956). Using an oxygen electrode we measured activation-induced changes in mitochondrial respiration of intact expanded human T cells. Treatment with agonistic anti-CD3 antibody or PMA resulted in inhibition of mitochondrial oxygen consumption (Figures 1A and S1A). Simultaneously, cellular uptake of radioactively labeled glucose (Figure 1B) and intracellular ATP level (Figure 1C) rose, highlighting a rapid shift toward a more aerobic glycolytic phenotype.

Upon TCR stimulation, a mitochondria-derived oxidative signal essential for activation-induced gene expression is generated (Figure S1B; Kamiński et al., 2007, 2010, 2012). To check a connection between the activation-induced metabolic shift and the oxidative signal, we tested the influence of 2-deoxyglucose (DOG) and 3-bromopyruvate (BrPyr), blockers of glucose metabolism, on the generation of TCR-induced ROS. After brief preincubation (30 min) with DOG/pyruvate, T cells generated lower amounts of activation-induced ROS compared to cells preincubated with equimolar concentrations of glucose (Glc)/pyruvate (Figure 1D). Treatment with the more potent inhibitor BrPyr resulted in complete block of TCR-induced ROS generation and NF-κB-dependent IL-2, IL-4, and IκBα gene expression (Figures 1E, 1F, S1C, and S1D). Both agents also reduced the intracellular oxidative background (Figure S1E).

Stimulation of the TCR Leads to Major Changes in Mitochondrial Bioenergetics and Ultrastructure

To investigate the relationship between the activation-induced metabolic shift and the mechanism of mitochondrial ROS release, we assessed the bioenergetic status of respiratory chain complexes. To this end, we applied snap-frozen and digitonin-permeabilized expanded T cells. As shown in Figure 1G (upper), TCR triggering resulted in a decrease of activity for complexes I and II, while activity of complex III was increased. A similar pattern could be observed after PMA treatment (Figure 1G, lower), showing independence from TCR-triggered mitochondrial Ca²⁺ uptake and involvement of a DAG/PKCθ-dependent pathway. In line with this notion, pretreatment of T cells with bis-indolyl-maleimidate I (BIM), an inhibitor of PKC and TCR-induced ROS generation (Kamiński et al., 2007), blocked the observed phenomena (Figures 1H, 1I, and S1F). The changes of enzymatic activity did not correspond to changes in the protein content of the complexes (Figure S1G) or their migration in BN-PAGE (Figure S1H). Interestingly, ultrastructure of mitochondria changed upon TCR or PMA triggering (Figure 2). Disarrangement and distortion of cristae were particularly pronounced in TCR-activated cells (Figure 2C), while PMA treatment led to various degrees of alteration (Figure 2B). No obvious rupture of outer and inner mitochondrial membranes could be detected. Since these changes occur rapidly after stimulation (1 hr) and are paralleled by the activation phenotype of cells (e.g., rise in ATP level, upregulation of glucose transport, and chromatin relaxation), an apoptotic origin was excluded. The alterations closely resembled those observed in highly glycolytic tumors and reported to occur as an adaptive response to hypoxia (Arismendi-Morillo, 2011) or to state IV of respiration (rate-limiting low ADP content and high ROS production) (Mannella, 2006). Thus, mitochondrial electron micrographs indicate low respiratory activity.

Next, we analyzed electron flow rates from complex I/II to complex III in either permeabilized cells or isolated mitochondria (Figure 1J). In the first case, T cell activation led to a decreased electron flow rate between complex I or II and complex III, in line with previous results (Figure 1G). Mitochondrial isolation abolished these effects and resulted in an enhanced electron flow toward complex III upon T cell activation (Figure 1J). These results suggest a transient character of activation-induced decrease of complex I/II activities (due to a labile agent) and a stable modification of complex III. The observed changes could be attributed to a hyperreduced state of ubiquinone, the electron carrier between complexes I/II and complex III (Lambert and Brand, 2009; Miwa et al., 2003). Accumulation of ubiquinol decreases activities of complex I and II by blocking the electron flow. This effect would be lost after isolation of mitochondria due to the oxidation of ubiquinol. Reverse electron transfer (RET), a major mechanism of mitochondrial ROS generation via complex I, is mediated by a highly reduced pool of ubiquinone (Lambert and Brand, 2009; Miwa et al., 2003). Ubiquinol accumulation is also crucial for ROS release at complex III or hyperglycemia/hypoxia-induced mitochondrial ROS generation (Bell et al., 2007; Nishikawa et al., 2000; Wellen and Thompson, 2010).

To investigate the role of the ubiquinone redox status for T cell activation, we tested the influence of different respiratory chain
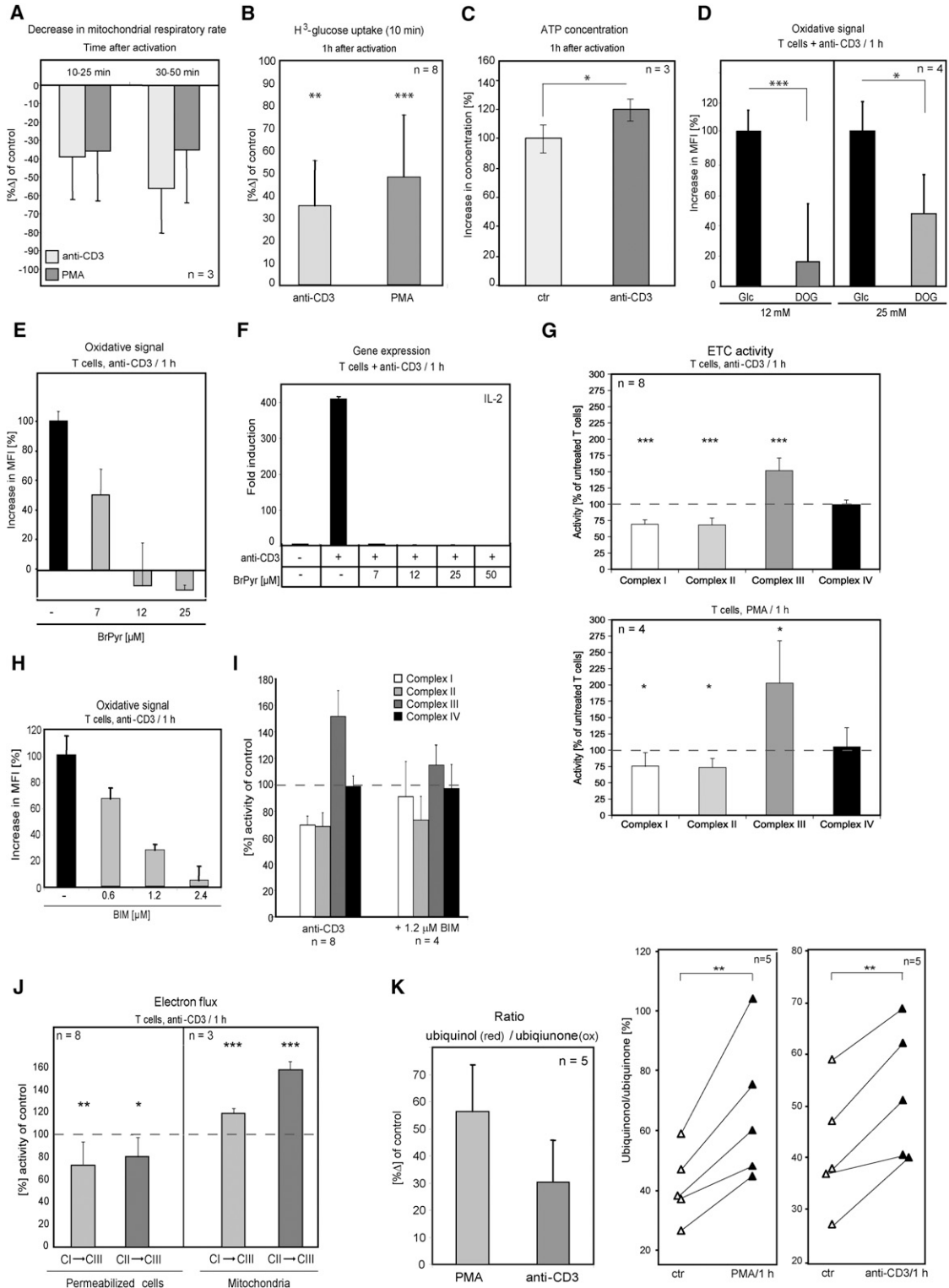
Figure 1. TCR-Induced Oxidative Signaling is Accompanied by a Rapid Metabolic Shift and Change in Mitochondrial Bioenergetics

(A) Respiratory rate of in vitro expanded peripheral T cells was monitored upon stimulation with soluble anti-CD3 antibody (10 μg/mg, GAM crosslinked) or PMA (10 ng/ml). Decrease in mitochondrial respiratory rate between control state (15 min prior to induction) and stimulated state (indicated time intervals for n = 3 donors).

(B) Uptake of D-[3-^{3}H] glucose measured in T cells 1 hr after activation (as in [A]). Results are shown as % of control ± SD (GAM – for anti-CD3; untreated – for PMA; n = 8 donors).

blockers on oxidative signal generation. The inhibition by complex-I-specific agents, rotenone and metformin (Kamiński et al., 2007, 2010), as well as moderate inhibition by complex II blockers, atpenin A5 and TTFA, suggest a RET-related mechanism of activation-induced mitochondrial ROS release (Figure S2A) (Batandier et al., 2006; Dröse et al., 2011; Dröse and Brandt, 2012; Lambert and Brand, 2009). Moreover, T cell activation-induced mitochondrial ROS generation was increased by inhibition of complexes III or IV (antimycin A or NaN$_3$, respectively). This could be due to a higher content of reduced ubiquinone, ROS release at complex I, and/or partial ROS release at complex III (Chowdhury et al., 2005; Dröse and Brandt, 2012; Tretter et al., 2007). Of note, the oxidative signal was unaffected by oligomycin, an ATP synthase inhibitor (Figure S2A). Essentially, these results recapitulated those previously reported for Jurkat cells (Kamiński et al., 2007). TCR triggering leads to rapid accumulation of NADH in the mitochondrial matrix, suggesting an abrogation of electron flow and hyperreduction of ubiquinone (Jones et al., 2007). Moreover, the detected endogenous complex IV activity in human T cells is about eight times lower than complex III activity (Figure S2B), forming a bottleneck for the regeneration of ubiquinone. Thus, we investigated ubiquinone redox status upon T cell activation. HPLC-based analysis of extracts from snap-frozen activated T cells revealed a significant rise in the content of ubiquinol over ubiquinone, reaching 30% and 57% upon TCR- and PMA-mediated triggering (Figure 1K), respectively, thus demonstrating a hyperreduced status of the ubiquinone pool after T cell activation.

Diverted Glycolytic Flow Leads to a GPD2-Mediated Mitochondrial ROS Release

In hyperglycemic or hypoxic cells, mitochondrial ROS production due to a hyperreduced ubiquinone pool is associated with an increased glucose metabolism (Bell et al., 2007; Nishikawa et al., 2000; Wellen and Thompson, 2010). Therefore, we measured activities of all major glycolytic enzymes upon TCR triggering (Figures 3A and 3B). The only enzymatic activity significantly changed was the reverse reaction of enolase (ENO) (Figure 3B). The reaction was blocked by NaF, an ENO inhibitor (Qin et al., 2006) and NaVO$_3$, an inhibitor of histidine phosphorylation (Krivanek and Novakova, 1991) (Figure S2C, left). Specific assay conditions (see Experimental Procedures) revealed that the increased enzymatic activity is an ATP-independent phosphoenolpyruvate (PEP) dephosphorylation of K$_m$ = 19.3 μM (Figure S2C, right). The dephosporylation of PEP shows substrate inhibition above 250 μM PEP and is mildly

inhibited by NaF and strongly blocked by NaVO$_3$ (data not shown).

The dimeric, low-affinity form of pyruvate kinase M2 (PK-M2) can dephosphorylate PEP in the absence of ADP and, moreover, is a functional protein kinase at low and physiological PEP levels (Gao et al., 2012). PK-M2 is highly expressed in activated T cells (Hruz et al., 2008; Netzker et al., 1992). In our hands, PK activity in T cells is approximately 10 times higher than the observed PEP dephosphorylation. It was also mildly affected by NaF and strongly reduced by NaVO$_3$ (only at low PEP concentrations, 100 μM). This suggests that the observed PEP phosphatase activity could be catalyzed by PK-M2.

Lower PK activity of the dimeric form PK-M2 results in a diminished metabolic flux through the GAPDH-initiated glycolytic pathway (Vander Heiden et al., 2010). Therefore, we analyzed metabolite flux downstream of GAPDH- and cytosolic glycerol-3-phosphate dehydrogenase (GPD1)-initiated branches of glycolysis (Figure 3A). TCR triggering clearly enhanced fructose-6-phosphate metabolism in the direction of GPD1, while the GAPDH-mediated turnover was slightly decreased (Figure 3C). In addition, production of lactate, the end-product of the GAPDH pathway, was decreased despite increased glucose uptake (Figures 1B and 3D).

To investigate whether this change of glycolytic flux impairs metabolic flow, we measured levels of glucose-6-phosphate and dihydroxyacetone phosphate upon TCR stimulation (Figure S2D). No alterations of glucose-6-phosphate levels were observed, indicating that the modification of the GAPDH-initiated branch leads neither to a reduced glycolytic rate nor to accumulation of initial glycolytic metabolites. Dihydroxyacetone phosphate levels were strongly reduced, indicating an increased glycolytic flux through the GPD shuttle.

Since glycerol-3-phosphate metabolism is crucial for T cell activation (Collison et al., 2008), we investigated the activity of cytosolic GPD1 and mitochondrial GPD2 upon TCR stimulation. GPD1 activity was unchanged, whereas activity of GPD2 was significantly upregulated (Figures 3B and 3E). PKC inhibition by BIM clearly blocked TCR-induced GPD2 activation (Figure 3E). PMA treatment also upregulated GPD2 activity (Figure 3E; mean activity was 0.19 ± 0.04 mU/mg protein for unstimulated T cells [n = 7 donors], 0.35 ± 0.14 mU/mg protein for anti-CD3-stimulated T cells [n = 7], and 0.24 ± 0.023 mU/mg protein for PMA-activated T cells [n = 3]). In contrast to a previous report (Tu et al., 1995), PMA treatment did not induce GPD1 activation (data not shown). Since Ca^{2+} binding lowers the K$_m$ of GPD2 for glycerol-3-phosphate, the TCR-induced Ca^{2+} signal could

---

(C) Increase in intracellular ATP content ± SD (cells activated as in [A] and [B]; ctr = 13.28 nmol/mg protein, n = 3 donors).

(D–F) Cells were stimulated for 1 hr with plate-bound anti-CD3 antibody (30 μg/ml). The oxidative signal after preincubation in PBS + 110 μg/ml pyruvate + Glc/DOG (30 min) (n experiments ± SD) (D) or in medium + BrPyr (20 min) (representative experiment) (E) is shown. (F) IL-2 expression in T cells treated as in (E).

(G–K) Cells were stimulated for 1 hr with anti-CD3 antibody (as in [D]) or PMA (as in [A]). After snap-freezing and permeabillization, steady-state enzymatic activities of ETC (electron transport chain) complexes were measured. (G) Results for n experiments/donors are shown as the percentage of untreated control (set to 100%, dashed line) ± SD. (H and I) For cells pretreated (20 min) with BIM oxidative signal generation (H) (representative measurement ± SD shown) or steady-state enzymatic activities (I) were measured (as in [G], n = 8 or n = 4 experiments/donors ± SD). (J) Electron flux from complex I (CI)/complex II (CII) to complex III (CIII) was measured in pemeabilized cells or mitochondrial fractions. Data for n experiments/donors ± SD are presented as in (G) and (I). Student's t test: p < 0.001 (***); p < 0.01 (**); p < 0.05 (*). (K) Cellular extracts were analyzed by HPLC. Change in ubiquinone redox status is shown as % difference between ubiquinonol/ubiquinone ratio of control cells (set to 0) and activated cells (mean ± SD for n = 5 experiments/donors) (left) and % ratio of ubiquinonol/ubiquinone concentration for each experiment/donor; paired Student's t test, p < 0.01 (**).
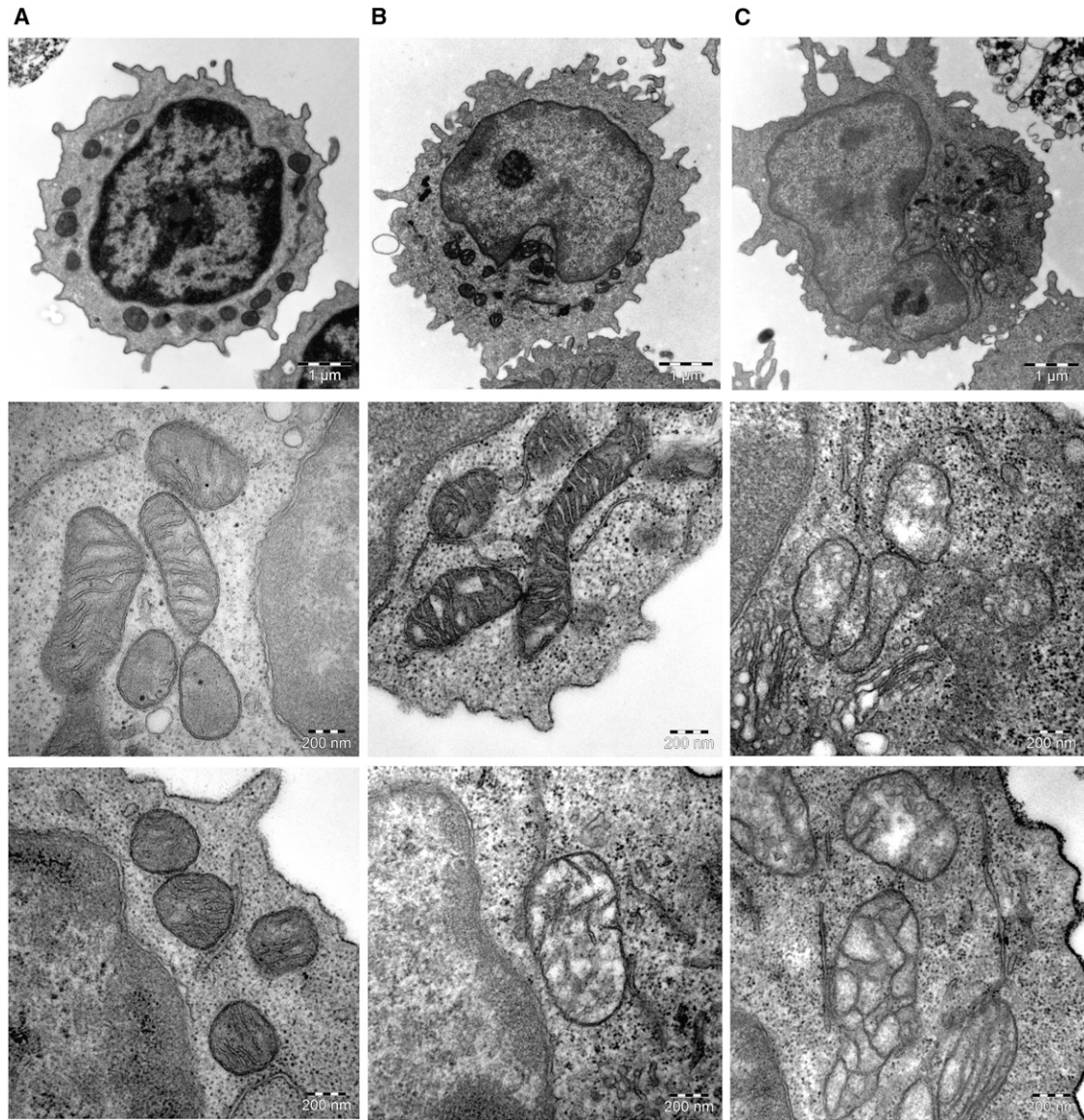
See also Figure S1.

Figure 2. Rapid ultrastructural changes of mitochondria upon activation

(A–C) In vitro expanded T cells were left untreated (A) or activated for 1 hr with PMA (B) or with plate-bound anti-CD3 antibody (as in Figures 1A and 1D, respectively) (C). Cells were subjected to electron microscopy. Representative images are shown. Scale bars, 1 μM (magnification 7000×) or 200 nM (magnification 50,000×).

potentiate PMA (DAG)-dependent activation of GPD2. However, Ca^{2+}-induced activation of GPD2 occurs already in the range of normal cytosolic Ca^{2+} concentrations (100 nM in resting T cells; GPD2 $k_{0.5}$ = 80–130 nM [Feske, 2007; Idahl and Lembert, 1995; Rutter et al., 1992]). Thus, a TCR-induced rise in Ca^{2+} concentration (up to 1 μM) could have rather moderate effects on GPD2.

Since GPD2 activity was indirectly detected via complex-III-mediated cytochrome *c* reduction, we verified our findings using 2,6-dichlorophenolindophenol as the direct electron acceptor. The obtained results confirmed the anti-CD3/PMA-dependent rise of GPD2 activity (Figure S2E). Moreover, the rise in GPD2 activity observed initially (1 hr) upon TCR triggering was still

present after 4 hr (Figure S2F). Thus, activation of GPD2 could also represent a major change in energy metabolism of activated T cells. To further investigate a role of glycerol-3-phosphate as the energy source for activated T cells, we tested the ability of 1 hr CD3-activated and subsequently digitonin-permeabilized cells to respire using glycerol-3-phosphate. Strikingly, NaCN-sensitive mitochondrial oxygen consumption was observed almost exclusively after T cell activation (Figure S2G).

GPD2 transfers electrons to the respiratory chain via reduction of ubiquinone. It has been shown that GPD2-sustained respiration induces mitochondrial ROS release. ROS could be released by GPD2 itself. In addition, GPD2-driven ROS production can be

blocked by rotenone and enhanced by inhibition of complexes III or IV. Thus, ROS originate also at complex I (due to RET), but a contribution of complex III could not be excluded (Chowdhury et al., 2005; Dröse and Brandt, 2012; Lambert and Brand, 2009; Miwa et al., 2003; Tretter et al., 2007). Next, we tested whether T cell activation-induced upregulation of GPD2 activity participates in mitochondrial ROS release.

Transient (siRNA-mediated) and stable (small hairpin RNA [shRNA]-mediated) knockdown (k.d.) of GPD2 expression in Jurkat T cells resulted in decreased generation of the oxidative signal (Figures 3F, 3G, S3A, and S3B). Consequently, transient downregulation of GPD2 inhibited PMA- or PMA/Iono-induced activation of an NF-κB luciferase reporter and led to diminished expression of IL-2 (Figure 3H and 3I). In addition, induction of IL-2 and IL-8 gene expression was also inhibited in cells stably transduced with lentiviral particles carrying anti-GPD2 shRNA (Figures S3C and S3D). Of note, shRNA-expressing cells changed the phenotype over time (during the third week of puromycin selection), lowering the extent of GPD2 k.d. and regaining the ability to generate ROS and express IL-2, but not IL-8, upon stimulation (data not shown). This is most likely due to the essential functions of GPD2 and IL-2 for T cell metabolism and proliferation.

To verify a causative link between decreased GPD2 expression, diminished oxidative signal, and activation-induced gene expression, we applied a previously established method utilizing glucose oxidase (GOX) as the exogenous source of a sustained, low, and physiologically relevant H_2O_2 signal (Gülow et al., 2005; Kamiński et al., 2010). H_2O_2 produced in medium crosses the plasma membrane and mimics the oxidative signal observed upon T cell activation (Figure S3E). When supplemented by Iono-triggered Ca^{2+} signal, this GOX-mediated H_2O_2 signal could partially restore IL-2 expression regardless of diminished GPD2 content (Figure S3F and S3G). In conclusion, T cell activation results in a diversion of the glycolytic flux toward GPD2, GPD2 activation, hyperreduction of ubiquinone, and ROS release.

TCR Triggering Activates a New ADP-Dependent Glucokinase

Glucose-induced hyperreduction of the ubiquinone pool and mitochondrial ROS release depend on an upregulated glycolytic flux (Nishikawa et al., 2000; Wellen and Thompson, 2010). However, enzymatic activities of the major glycolytic regulatory steps, hexokinase (HK), phosphhofructokinase (PFK), glyceraldehyde 3-phosphate dehydrogenase (GAPDH), and pyruvate kinase (PK) (Figure 3A), were unchanged after TCR triggering (Figure 3B). Association of HK with mitochondrial VDAC abolishes end-product inhibition of HK and acts as yet another mechanism for glucose flux upregulation (Wilson, 2003). Western blot (WB) analysis of mitochondria-enriched membrane fractions of expanded T cells revealed high HK1 and low HK2 levels (Figure S4A). Nevertheless, TCR triggering did not lead to recruitment of HK1/2 to mitochondria or upregulation of mitochondria-associated HK activity (Figures S4A and S4B). Next, we investigated mitochondria-associated HK activity coupled to respiration-mediated ATP generation (Figure S4C). TCR triggering induced an HK-like activity in the presence of ADP and

succinate in the "high g" mitochondrial fractions (Figure S4D). This activity was only mildly blocked by the adenylate kinase (AK) inhibitor diadenosine pentaphosphate (Ap5A, 5 μM, up to 20%–40% inhibition), whereas mitochondrial AK was strongly inhibited (80%–90% inhibition). The stimulation-induced rise in HK-like activity was unaffected by Ap5A (data not shown). Surprisingly, this activity was independent of succinate, but dependent on ADP. Insensitivity to the complex IV inhibitor NaCN and the uncoupler carbonylcyanide m-chlorophenylhydrazone (CCCP) demonstrated independence from mitochondrial ATP production (Figure S4D).

The ADP-dependent glucokinase (ADPGK) phosphorylates glucose by utilizing ADP (Richter et al., 2012; Ronimus and Morgan, 2004). Although typical for thermophilic Archaea, ADPGK exists in mammals and is highly expressed in human hematopoietic cells, including T cells (Hruz et al., 2008; Wu et al., 2009). WB analysis revealed a high ADPGK content in T cells and Jurkat cells (Figures 4A and 6E). A lack of end-product inhibition provides ADPGK with the ability to potentiate the glycolytic flux (Ronimus and Morgan, 2004). Of note, enhanced ADPGK activity occurred in high g mitochondrial fractions from anti-CD3-treated T cells. Comparable upregulation of activity could be achieved by PMA treatment of T cells or Jurkat cells (Figure 4A), indicating independence from Ca^{2+}-mediated TCR signaling (Figure 4A; mean activity 0.67 ± 0.30 mU/mg protein for unstimulated T cells [n = 14 donors], 1.07 ± 0.32 mU/mg protein for anti-CD3-stimulated T cells [n = 8], and 1.00 ± 0.11 mU/mg protein for PMA stimulated T cells [n = 4]). Consistently, the increase of ADPGK activity was completely abolished by BIM (Figure 4A).

ADPGK was present in high g mitochondrial (mostly membrane components) but not in cytosolic fractions (Figures 4B, S4E, and S4F). No upregulation of ADPGK content upon TCR stimulation could be found (Figure 4B). T cell activation-induced upregulation in ADPGK activity and ROS generation were independent of de novo gene expression, as demonstrated by actinomycin D treatment (Figures S4J–S4L).

Interestingly, the ADPGK sequence contains a putative signal peptide for transport into the endoplasmic reticulum (ER) (Figures 5C, S5A and S5D) (UniProt Q9BRR6). Since T cell mitochondria are smaller than the ones of other tissues (e.g., liver), we utilized an 11,000 × g centrifugation step to increase the yield of mitochondria in high-g mitochondrial fractions. Such fractions also contain ER, as demonstrated by electron micrographs (data not shown) and WB (Figure 4B). To investigate subcellular localization of ADPGK, we prepared "mitochondria-enriched" and "ER-enriched" fractions (see Experimental Procedures) demonstrating a possible ER association of ADPGK in T cells and Jurkat cells (Figures S4E and S4F). Next, we purified ER particles from Jurkat cells by density-gradient ultracentrifugation. ADPGK protein content and activity closely correlated with the ER markers: calreticulin (WB), NADPH cytochrome c reductase (enzymatic activity), and glucose-6-phosphatase (G6Pase, enzymatic activity) (Figures 4C, 4D, and S4G–S4I). Activation-induced increase in ADPGK activity was also ER-confined (Figure S4H). Intracellular ADPGK localization was further examined by confocal immunofluorescence microscopy using HEK293T cells overexpressing ADPGK tagged with
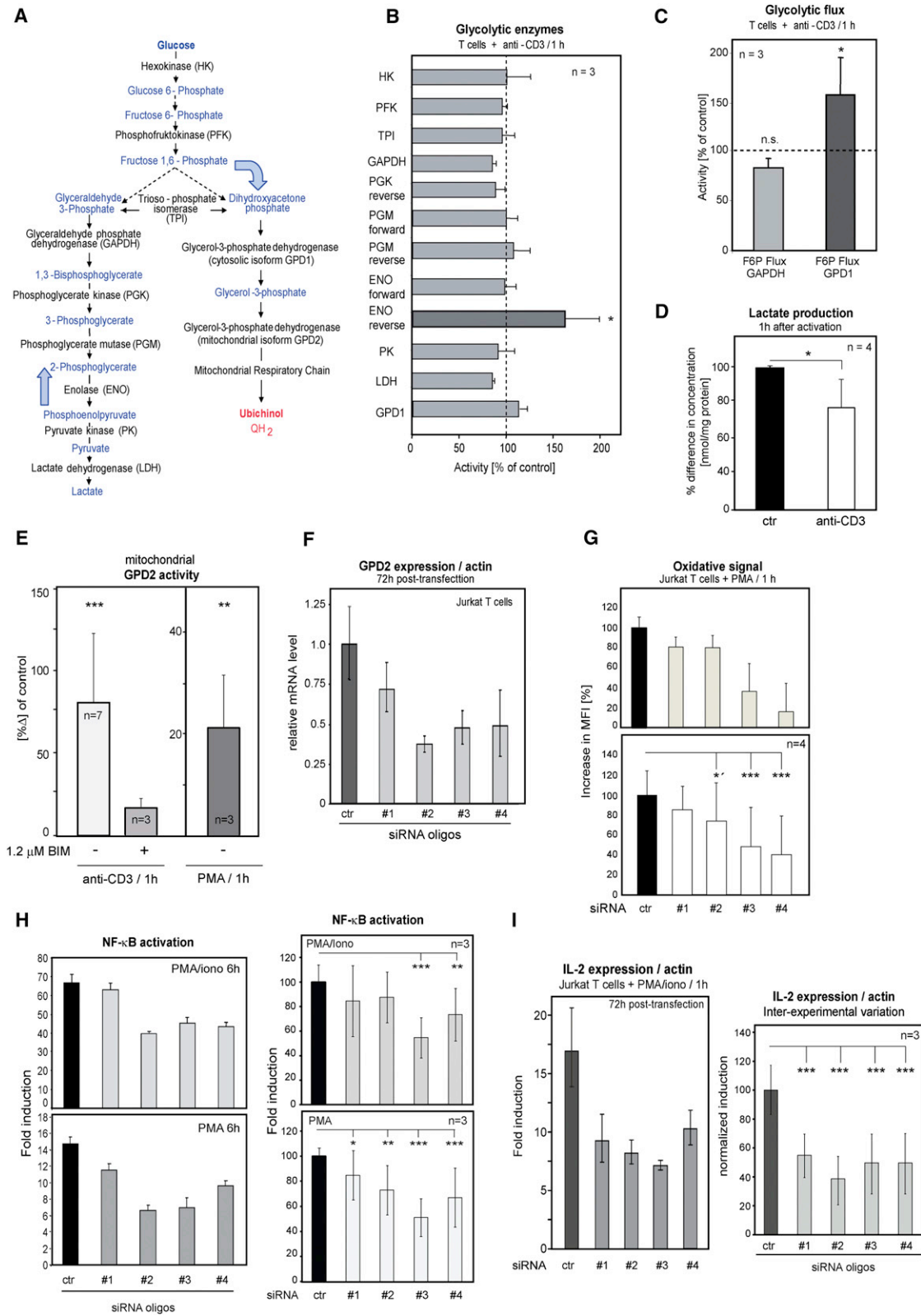
Figure 3. T Cell Activation Diverts the Glycolytic Flux toward Mitochondrial GPD Shuttle

(A) The glycolytic pathway (block arrows indicate the diverted metabolic flow). Expanded T cells were stimulated for 1 hr with anti-CD3 antibody that was plate-bound (B, C, and E), as in Figure 1D, or soluble crosslinked (D), as in Figure 1A.

turboGFP (tGFP, C terminus). Micrographs clearly demonstrate colocalization of the tGFP-specific signal with staining for the ER marker, calnexin (Figures 4E and 4F). In conclusion, the predicted signal sequence, results of subcellular fractionation, and confocal imaging indicate ER localization of ADPGK.

Lack of ADPGK in cytosolic fractions (Figure 4B, S4E, and S4F) suggested ER-membrane association of ADPGK. Interestingly, the existence of a highly hydrophobic amino acid (aa) stretch (approximate position 80–100 aa) resembling a single membrane-spanning region downstream of the signaling peptide was predicted (Figures S5A and S5D). Moreover, the initial part of this region demonstrates properties of an amphipathic helix (Figures S5B and S5D), further suggesting membrane association.

To better understand the metabolic role of ADPGK, we investigated whether its active site is positioned toward the cytosol or the ER lumen. Activities of ADPGK and G6Pase (an ER enzyme with the active site protruding into the ER lumen) were measured in ER particles prepared by density gradient ultracentrifugation with or without 0.1% digitonin. Upon addition of digitonin, G6Pase activity increased 1.6 times due to increased substrate availability. In contrast, digitonin did not affect ADPGK activity indicating positioning of the active site toward the cytosol (Figure 5A). Orientation of the ADPGK active site was further analyzed by protease protection assay. Fractions of ER particles were either (1) left untreated, (2) treated with trypsin, or (3) treated with trypsin and detergent. To map the active site of ADPGK, we utilized a monoclonal antibody recognizing an aa stretch at positions 425–497 covering the active site (475–484 aa, C terminus) (Figure S5D). Trypsin digestion completely abolished the WB ADPGK signal, while the signal for calreticulin (a protein of ER lumen) was strongly reduced in the case of detergent-treated samples (Figure 5B). Our results suggest that cytosolic orientation of the active site enables participation of ADPGK in the regulation of glycolytic flow upon T cell activation. The experimental approaches used and putative positioning of ADPGK in the ER membrane are depicted in Figure S5C.

Using ER-enriched fractions from TCR-triggered T cells, we found that ADPGK activation is an early and transient event in the course of a TCR-induced response (Figure S6A). The rise in ADPGK activity is in close temporal correlation with oxidative signal generation (peaks within 1–2 hr upon TCR stimulation and declines thereafter) and the resulting induction of gene expression (Kamiński et al., 2012). ADPGK activity in ER-enriched fractions was also characterized in terms of kinetic parameters. It revealed a striking pH optimum of 6.0 and a K_m for glucose of 0.086 mM (pH 6.0, 37°C). These values resemble the ones reported for recombinant mouse ADPGK (Ronimus and Morgan, 2004). Interestingly, recently reported recombinant human ADPGK demonstrated a K_m for glucose of 0.29 mM (Richter et al., 2012). In our studies, substrate affinity was similar to so-called low-K_m HKs 1–3. ADPGK was substrate-inhibited at glucose concentrations higher than 5 mM.

Next, we generated Jurkat cells stably expressing ADPGK protein with an N-terminal FLAG tag (F-ADPGK Jurkat cells; Figure 5C). As for wild-type ADPGK protein (WT-ADPGK), the FLAG-ADPGK protein (F-ADPGK) was found in the ER-enriched fractions (Figure S4E) and was copurified with ER particles (Figure S4G). Cells expressing F-ADPGK showed higher basal and enhanced PMA-induced ADPGK activity compared to control cells (Figure 5C). Immunoprecipitated FLAG-ADPGK protein demonstrated ADPGK activity, absent in precipitates from control lysates (Figure 5D, lower). The results were confirmed by WB (Figure 5D, upper). Thus, an active endogenous human ADPGK could be demonstrated. Of note, F-ADPGK Jurkat cells exhibited increased glucose uptake (Figure S6B). siRNA-mediated k.d. of HK1 did not affect the elevated glucose import, indicating that ADPGK takes part in glucose metabolism (Figures S6C and S6D).

In addition, we assayed the effects of DOG and BrPyr (each 5 mM) on purified F-ADPGK. At nonsaturating glucose concentration (1 mM), DOG increased F-ADPGK activity, indicating production of DOG-6-phosphate (as described for classical HKs; DOG-6-phosphate inhibits glucose-6-phosphate isomerase) (Wick et al., 1957). BrPyr strongly inhibited ADPGK (Figure S6E).

The secondary structure prediction for mammalian ADPGK revealed a high structural similarity to the known secondary structure of thermostable archaeal ADPGK, despite a low sequence homology (Figure S5D) (Tsuge et al., 2002). Therefore, we tested temperature dependence of ADPGK activity in ER-enriched fractions from T cells. As shown in Figure S5E, velocity of the ADPGK-catalyzed reaction exponentially increased within the physiological temperature range and was 3.5 times higher at 42°C than at 37°C. In contrast, the temperature-driven rise in HK activity remained linear. Furthermore, at 42°C the velocity of the ADPGK-mediated reaction was comparable to that of HK. In conclusion, TCR triggering transiently and in a PKC(DAG)-dependent way activates ADPGK, a thermostable, ER-associated glucose-phosphorylating enzyme without end-product inhibition.

(B) Status of glycolytic enzymes upon T cell activation (for acronyms, see [A] and text). Results are shown as % of untreated control (set to 100%, dashed line), for n = 3 experiments/donors ± SD.

(C) Fructose-6-phosphate (F6P) metabolic flux toward GPD1/GAPDH measured in the cytosol of activated T cells. Activation and data presentation are as in (B).

(D) Change in lactate concentration; n = 4 experiments/donors ± SD.

(E) Change of GPD2 activity in mitochondrial fractions of activated T cells ± 20 min pretreatment with BIM, shown as % of nonstimulated control; n experiments/donors ± SD.

(F) qRT-PCR analysis of siRNA-mediated GPD2 k.d. in Jurkat cells.

(G–I) After GPD2 k.d., Jurkat cells (G and I) or Jurkat cells stably expressing NF-κB-luciferase reporter (H) were activated with PMA (10 ng/ml) ± Iono (1 μM) and oxidative signal (G), NF-κB activation (H), or IL-2 expression (I) were assayed. Data are presented as representative triplicate experiments or interexperimental variation of downregulation for n experiments ± SD (induction of control cells set to 100%). Student's t test: p < 0.001 (***); p < 0.01 (**); p < 0.05 (*), p = 0.05 (*′) for #2 in H; n.s., nonsignificant.
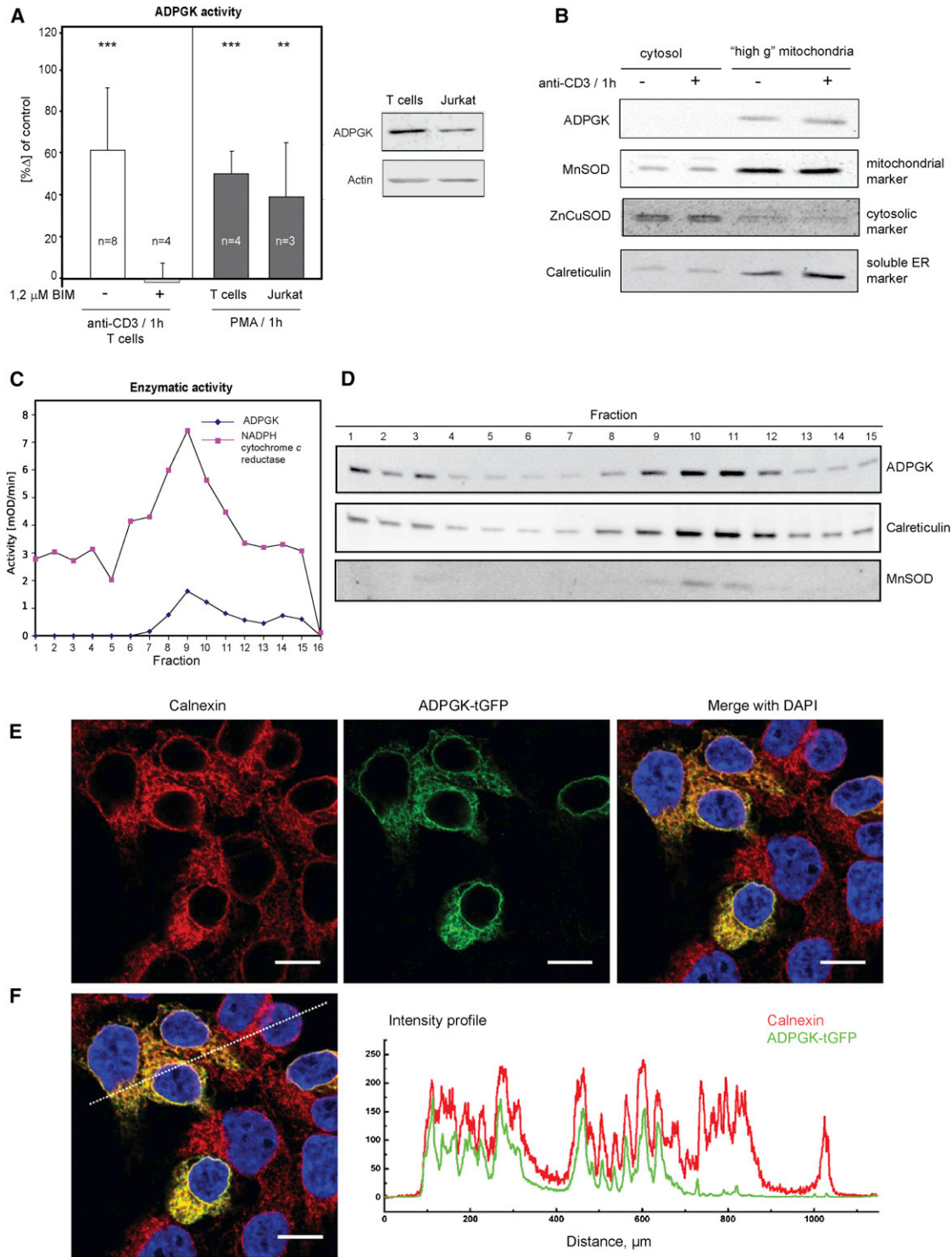
See also Figures S2 and S3.

Figure 4. T Cell Activation Triggers ADPGK, an ER-Localized Enzyme

(A and B) Expanded T cells or Jurkat cells were stimulated for 1 hr with plate-bound anti-CD3 antibody or PMA (as in Figure 2). (A) Left: ADPGK activity in mitochondrial high-g fraction (contains ER) of activated T cells or Jurkat cells ± 20 min pretreatment with BIM. Results for n experiments/donors shown (% increase over untreated control ± SD). Right: levels of ADPGK in lysates of T cells or Jurkat cells. Student's t test: $p < 0.001$ (***); $p < 0.01$ (**).

(B) WB analysis of mitochondrial (high g) and cytosolic fractions of activated T cells.

(C and D) ER particles were purified from Jurkat cells. In (C), enzymatic activities of ADPGK and NADPH cytochrome *c* reductase (ER marker) were measured.

(D) WB analysis for ADPGK, calreticulin (ER marker), and MnSOD (mitochondrial marker).
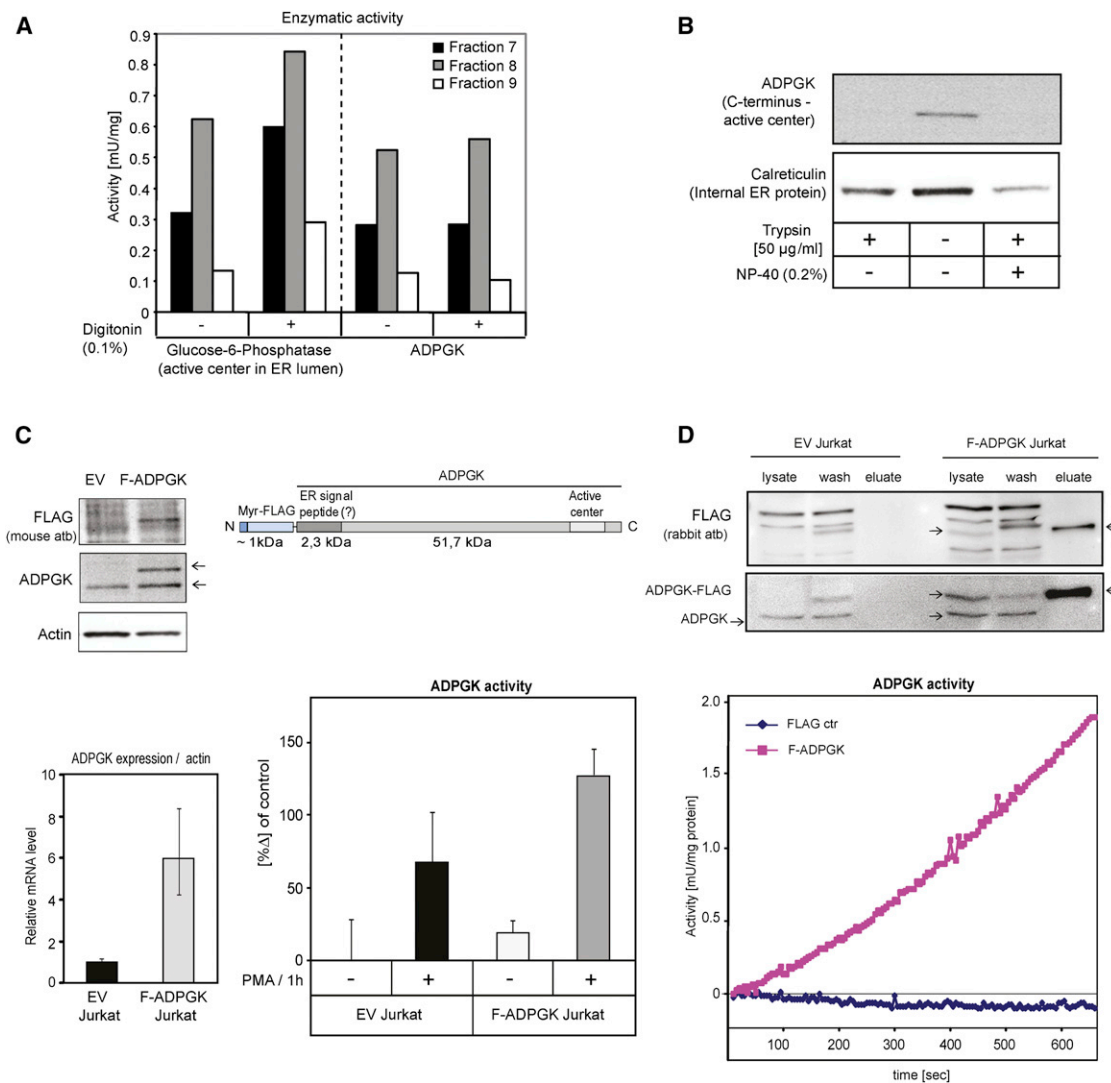
Figure 5. ADPGK has cytoplasm-oriented topology and is active upon overexpression

(A and B) Localization of ADPGK active site in ER particles purified from Jurkat cells. (A) ADPGK and glucose-6-phosphatase activities measured ± 0.1% digitonin.

(B) WB analysis of ADPGK (epitope encompassing enzymatic active site; calreticulin, luminal control) in ER particles after trypsin treatment (30 min, 50 μg/ml) ± 0.2% NP-40.

(C) Expression of the FLAG-ADPGK construct in Jurkat cells (F-ADPGK Jurkat, EV Jurkat, empty vector control). Left: WB (arrows, F-ADPGK and ADPGK) and qRT-PCR analyses of (F-)ADPGK content and expression. Right, upper: retroviral construct. Right, lower: ADPGK activity in ER-enriched fractions of activated F-ADPGK and EV Jurkat cells. Representative triplicated experiment ± SD (presented as in Figure 4A; activity for untreated EV Jurkat cells set to 0).

(D) Upper: WB of immunoprecipitated F-ADPGK (arrows, F-ADPGK and ADPGK proteins; FLAG WB, rabbit anti-FLAG antibodies; ADPGK WB, mouse antibodies, upper band on ADPGK WB in EV Jurkat "wash" line, H chain of mouse anti-FLAG [M2] antibody). Lower: ADPGK activity in immunoprecipitates ("eluate").

See also Figures S5 and S6.

ADPGK Mediates Generation of the Oxidative Signal

Next, we assayed the influence of lowering ADPGK expression by transient transfection with siRNA or stable transduction with shRNA-carrying retroviral or lentiviral particles on activation-induced ROS generation. ADPGK k.d. (Figures 6A and S7A–S7D) inhibited PMA-triggered production of ROS in Jurkat cells

(E) Confocal imaging of HEK293 cells expressing ADPGK-tagged with turboGFP on C terminus (ADPGK-tGFP) – cells stained with antibodies against tGFP and calnexin (ER membrane marker). Colocalization indicated by yellow color in merged images. Scale bar, 10 μm.

(F) Colocalization control, intensity profile of a section (dashed line).
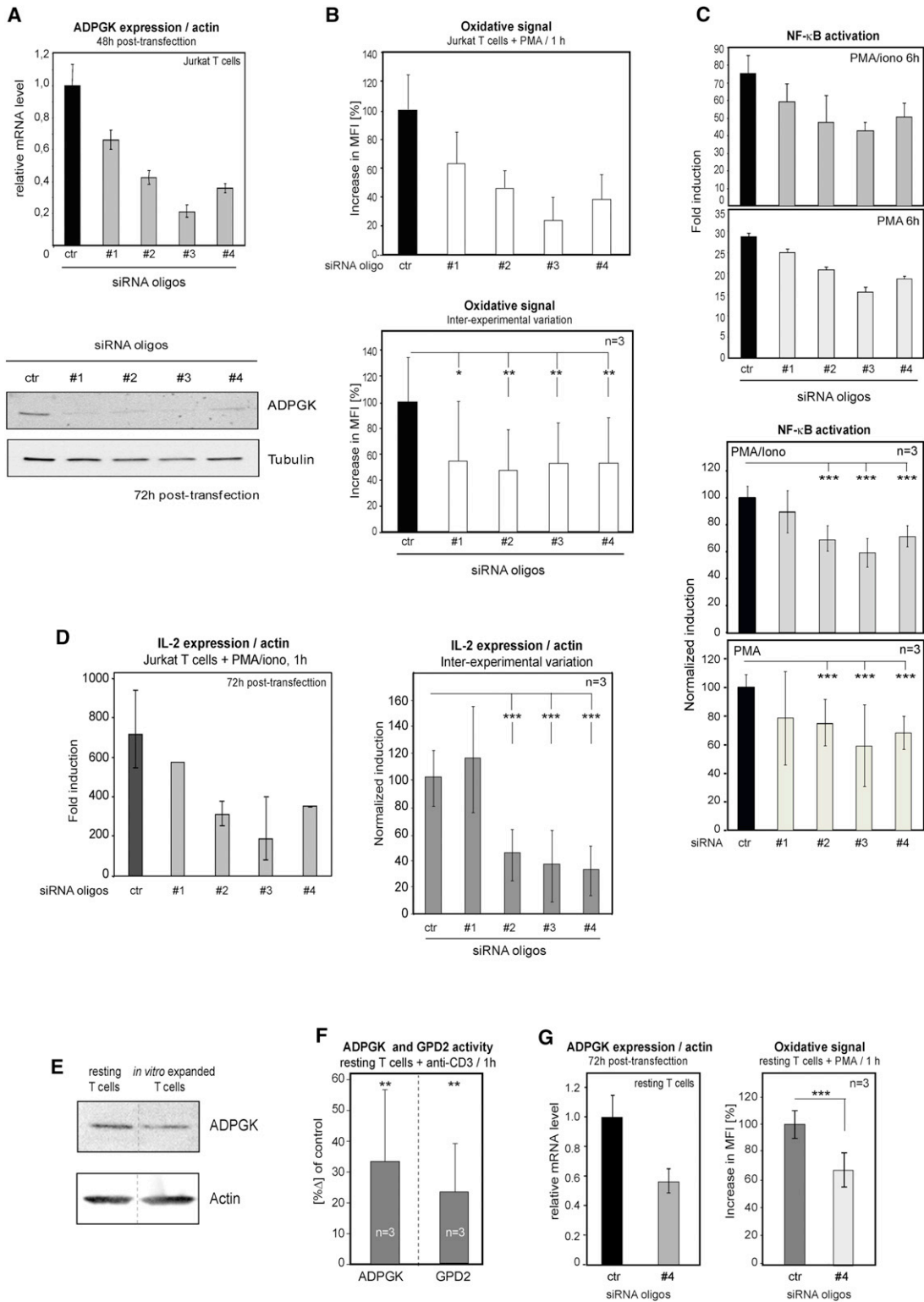
See also Figures S4 and S5.

Figure 6. Lowered ADPGK content inhibits activation-induced oxidative signal generation and gene expression

(A) ADPGK expression and content were analyzed in siRNA-transfected Jurkat cells by qRT-PCR and WB.

(B–D) After ADPGK k.d., Jurkat cells (B and D) or Jurkat cells stably expressing NF-κB-luciferase reporter (C) were activated with PMA ± Iono (as in Figures 3G–3I), and oxidative signal generation (B), NF-κB activation (C), or IL-2 expression (D) were analyzed. Representative experiments (B, C [upper], and D [left]) or interexperimental comparison ± SD (induction of control cells set to 100%) (B, C [lower], and D [right]) are presented.
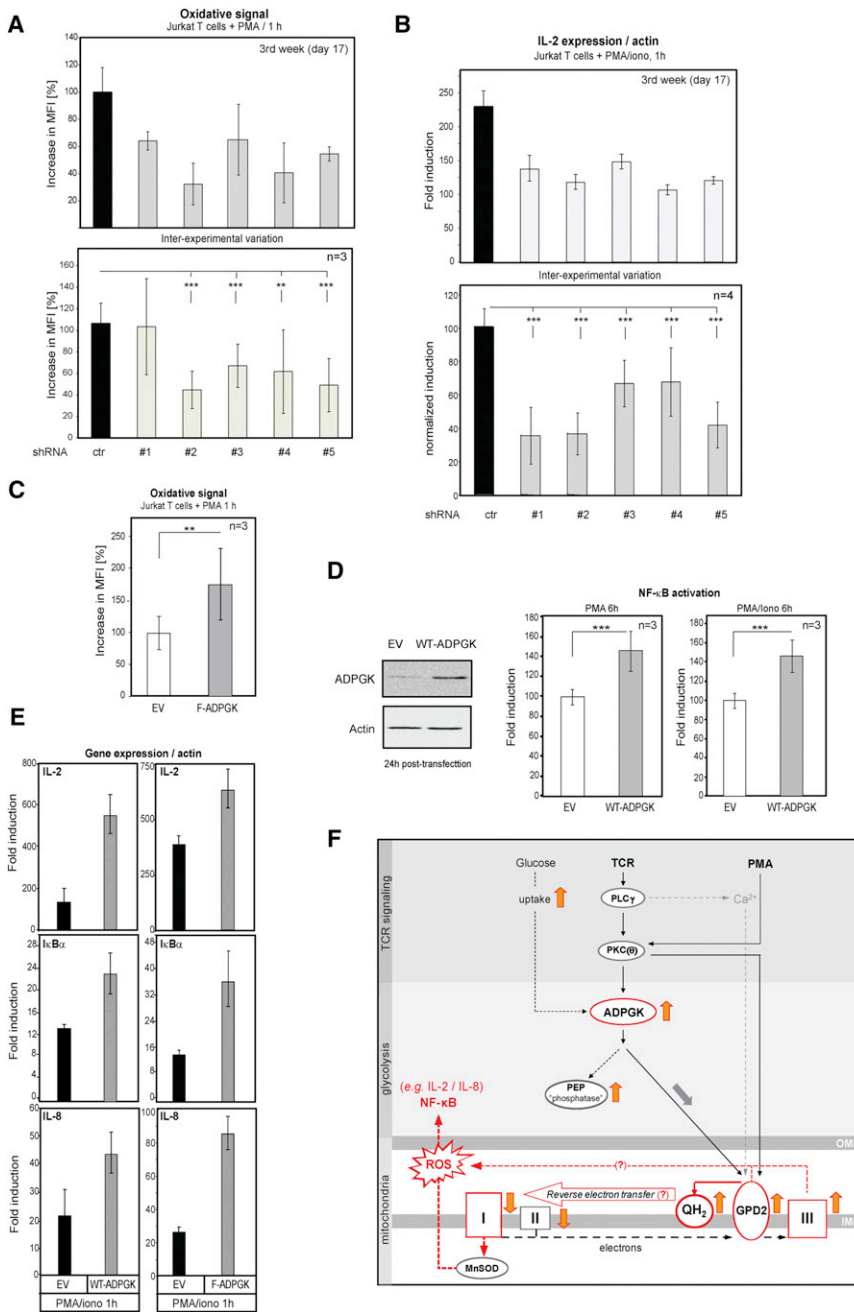
Figure 7. ADPGK Participates in Activation-Induced Oxidative Signal Generation and NF-κB Response

(A and B) Jurkat cells were transduced with lentiviral particles carrying shRNA against ADPGK (or nonsilencing control) and cultured with puromycin (1 μg/ml) for 3 weeks (for stability of ADPGK k.d. see Figure S7). Cells were activated for 1 hr with PMA ± Iono (as in Figures 3G–3I), and either oxidative signal generation (A) or IL-2 expression (B) were analyzed. Upper, results of single representative experiments (selection day 17). Lower, interexperimental variations of experiments performed during selection period (induction of control cells set to 100%); Student's t test: p < 0.001 (***).

(C–E) Jurkat cells stably expressing FLAG-ADPGK (F-ADPGK) proteins (C and E) or Jurkat cells (E) and NF-κB-luciferase reporter Jurkat cells (D) transiently overexpressing WT-ADPGK protein for 24 hr. (D) and (E) were activated with PMA ± Iono (as in Figures 3G–3I) for 1 hr (C and E) or 6 hr (D). Thereafter, oxidative signal (C), NF-κB activation (D), and IL-2, IL-8, or IκBα expression (E) were analyzed. Interexperimental variations of n experiments ± SD are presented (response of EV control cells set to 100%). (D) shows WB analysis of transient WT-ADPGK overexpression.

(F) Scheme of described pathway. Block arrows: orange, changes in enzymatic activity, transport (glucose), or ubiquinol content; gray, direction of diverted metabolic flux.

See also Figures S6 and S7.

phenotype of shRNA-transduced Jurkat cells was stable during the entire period of selection (2–4 weeks) for retroviral and lentiviral transductions. The exogenous oxidative signal introduced by addition of GOX (Figure S3E) partially recovered activation-induced IL-2 expression in siRNA- or shRNA-treated cells (Figures S7G and S7H). Thus, ADPGK-dependent ROS production is crucial for TCR-induced gene expression.

"Resting," nonexpanded human T cells also generate the oxidative signal from mitochondria (Kamiński et al., 2010). Likewise, activation of such T cells led to a rise

(Figures 6B, 7A, and S7E). Concomitantly, it resulted in inhibition of PMA- or PMA/Iono-triggered NF-κB activation (Figure 6C) and NF-κB-dependent expression of IL-2, IL-8 and IκBα genes (Figures 6D, 7B, S6F, S7C and S7F). The observed inhibitory

in GPD2 and ADPGK enzymatic activities (Figure 6F). Low-activity induction corresponds to a lower extent of ROS generation in resting T cells (Kamiński et al., 2010). siRNA-mediated k.d. of ADPGK expression decreased the activation-induced

(E) ADPGK protein levels in resting and expanded human T cells.
(F) Change of ADPGK and GPD2 activity in high-g mitochondrial fractions of resting T cells stimulated with plate-bound anti-CD3 antibodies (as in Figure 1D). Results for n experiments/donors shown as % of nonstimulated controls ± SD.
(G) Left, qRT-PCR analysis of siRNA-mediated k.d. of ADPGK expression in resting T cells. Right, after ADPGK k.d., T cells were stimulated with PMA, as in (B), and the oxidative signal was measured for n experiments/donors. Student's t test: p < 0.001 (***); p < 0.01 (**); p < 0.05 (*).
See Figures S6 and S7.

oxidative signal (Figure 6G), but the effects on gene expression will be subject to further study.

Furthermore, enhanced PMA-induced ADPGK activity in F-ADPGK Jurkat cells (Figure 5C) led to increased ROS production followed by potentiated induction of NF-κB-dependent genes (IL-2, IL-8, and IκBα [Figures 7C and 7E]). Similar results were obtained for Jurkat cells transiently overexpressing WT-ADPGK (Figures 7D and 7E), where induction of NF-κB and NF-κB-dependent gene expression were enhanced. Changes were more pronounced for IL-8 and IκBα than for IL-2 (Figure S6G). ADPGK overexpression tends to decrease basal transcript levels of NF-κB-dependent genes by an as yet unknown mechanism (Figure S6H). Thus, we demonstrate a novel role of mammalian ADPGK for T cell activation and a new connection between glucose metabolism, ROS generation, and cell signaling (Figure 7F).

DISCUSSION

T cell activation leads to a metabolic shift from mitochondrial respiration toward aerobic glycolysis (Wang et al., 1976). This so-called "Warburg phenotype" is a characteristic feature of fast-proliferating normal, but also malignant, cells (Vander Heiden et al., 2009; Warburg, 1956). Moreover, TCR triggering induces a mitochondrial oxidative signal contributing to NF-κB and AP-1 activation and subsequent gene expression (Jones et al., 2007; Kamiński et al., 2007, 2010, 2012; Yi et al., 2006). Upregulation of glycolysis upon hyperglycemic or hypoxic conditions increases mitochondrial ROS generation (Bell et al., 2007; Nishikawa et al., 2000; Wellen and Thompson, 2010). Thus, we studied the interplay of mitochondria and glycolysis upon T cell activation.

Here we show that T cell activation-induced mitochondrial ROS production and NF-κB-driven gene expression depend on activation of ADPGK, a protein typical for *Archaea* whose function in eukaryotes was unknown. TCR triggering upregulates glycolytic flux due to activation of ADPGK, an enzyme lacking end-product inhibition by glucose-6-phosphate, in contrast to classical HKs (Ronimus and Morgan, 2004). ADPGK activation is accompanied by a rapid glucose uptake, downregulation of mitochondrial oxygen consumption, and deviation of glycolysis toward the GPD shuttle. In turn, activation of GPD2 leads to a hyperreduction of ubiquinone and ROS release from mitochondria (Figure 7F). This is paralleled by major changes in mitochondrial bioenergetics and ultrastructure. It is worth noting that all events occur within 1 hr after TCR stimulation. Downregulation of ADPGK or GPD2 abundance inhibits oxidative signal generation and induction of NF-κB-dependent gene expression, whereas overexpression of ADPGK potentiates them.

Interestingly, mitochondrial respiration was decreased upon TCR triggering, while activity of complex IV, the major oxygen sink, was unchanged. However, shifting mitochondria to glycerol-3-phosphate respiration bypasses complex I/II and reduces electron flow to complex IV, i.e., the driving force of mitochondrial oxygen consumption (Tretter et al., 2007). A similar observation was made in CHO cells overexpressing GPD1 (Doherty et al., 1998). Alternatively, mitochondrial respiration may be inhibited by increased intracellular glucose concentration (Crab-

tree effect), which was reported to occur after T cell activation (Guppy et al., 1993).

It has been shown that glycerol-3-phosphate-supported respiration and GPD2 activation lead to ROS release (at GPD2 and/or complex I via RET) (Lambert and Brand, 2009; Miwa et al., 2003; Tretter et al., 2007). The TCR-induced oxidative signal depends on intact complex I and GPD2 activation and coincides with hyperreduction of ubiquinone. This suggests a RET-mediated mechanism of ROS release at complex I. However, effects of antimycin A and NaN₃, as well as upregulation of complex III activity, could also indicate an additional contribution of ROS release at complex III (Figure S2A). In this study, we applied predominantly dichlorofluorescin diacetate (DCF-DA) staining to monitor intracellular redox changes originating from the mitochondria (the oxidative signal acts in cytoplasm or nucleus to activate transcription). This limits conclusions regarding the enzymatic source of ROS. Of note, TCR-induced increase in mitoSOX fluorescence and the inhibitory effect of MnSOD indicate a rise in matrix superoxide concentration.

Interestingly, since GPD2 can functionally interact with complex III (Cottingham and Ragan, 1980), TCR-triggered stable activation of GPD2 may also lead to lowering of complex I/II activity with simultaneous rise in complex III activity (as observed in Figure 1G) via a common putative mechanism of GPD2 and complex III activation.

In our study, TCR triggering induced a PEP phosphatase activity that may have been catalyzed by a dimeric PK-M2. In proliferating cells, PK-M2 uses PEP as a phosphate donor and can act as a protein kinase of broad specificity (Gao et al., 2012). Furthermore, in PK-M2-expressing cells (Vander Heiden et al., 2010), an unknown protein able to use PEP for phosphorylation of a histidine residue of phosphoglycerate mutase was reported (Vander Heiden et al., 2010) (inhibition of reversed ENO reaction or PEP "unknown" phosphatase by NaVO₃; Figure S2C or data not shown, respectively).

Low PK activity of PK-M2 results in redirection of the glycolytic flux in favor of metabolic precursor synthesis (Vander Heiden et al., 2010). After TCR activation, we observed a similar redirection of glycolysis, as demonstrated by reduced lactate production and increased glycerol-3-phosphate shuttle activity. Redirection of glycolysis at the stage of PK-M2 omits one step of glycolytic ATP generation. Thus, induction of ADPGK and the use of PEP for protein phosphorylation may overcome this energetic drawback.

Data regarding expression profiling of human tissues indicate that ADPGK is preferentially expressed in cells of hematopoietic lineage, such as macrophages, monocytes, dendritic cells (DCs), T cells, and B cells (Hruz et al., 2008; Wu et al., 2009). This suggests a role for ADPGK in processes of activation-induced differentiation/division, which involve rapid demand for ATP, e.g., for signaling phosphorylation and cytoskeletal remodeling. Of note, it has been recently reported that Toll-like-receptor (TLR)-mediated DC activation is accompanied by a switch to aerobic glycolysis (Krawczyk et al., 2010).

Immune cell activation accompanies inflammation. Enhanced ADPGK activity in a proinflammatory temperature range (37°–42°C) (Figure S5E) may enable its functionality at the inflammatory site as mediator of a NF-κB-dependent response.

The close similarity between the predicted secondary structure of human ADPGK and crystal structure of ADPGK of thermophilic archaebacterium (Figure S5D) is indicative of thermostability of ADPGK (Tsuge et al., 2002).

Localization of ADPGK in the ER is an interesting issue. Positioning of the FLAG peptide on the N terminus (C terminus encompasses ADPGK active site; Figure S5D) does not interfere with ER localization and also leaves the protein fully active and responsive to a TCR/PMA (DAG)-mediated stimulus. Lack of detectable ADPGK protein in cytosolic/soluble fractions (Figures 4B, S4E, and S4F) suggests its membrane association. This is supported by prediction of a highly hydrophobic amino acid stretch (approximate position 80–100 aa) resembling a single membrane-spanning region (Figure S5A) or allowing the formation of a membrane-associated amphipathic helix (Figure S5B). The active site of ADPGK seems to protrude into the cytoplasm (Figures 5A and 5B). This feature indicates a possible role for ADPGK in cytosolic glucose metabolism.

Cancer cells often display a Warburg phenotype and are endowed with high intrinsic ROS production and constitutive activation of the NF-κB pathway (Baud and Karin, 2009; Wellen and Thompson, 2010). Thus, the described interplay of signaling and metabolic pathways resulting in mitochondrial ROS release may have a meaning for tumorigenesis.

In conclusion, we provide experimental evidence for an unexpected role for ADPGK as a novel regulator of T cell activation. In addition, based on the identified mechanism of glycolytic-flux-induced mitochondrial ROS release for T cells, we propose a hypothesis connecting the increased aerobic glycolysis (e.g., Warburg phenotype) with increased mitochondrial ROS levels and enhanced NF-κB signaling.

EXPERIMENTAL PROCEDURES

ADPGK Activity Assay
NADP reduction was monitored in an ETC buffer containing 1 mM ADP, 1 mM glucose, 0.5 mM NADP, 5 μM Ap5A, and 0.05 U/ml glucose-6-phosphate dehydrogenase at pH 6.0 and 37° or 42°C. Assay conditions based on those previously described for recombinant mouse ADPGK (Ronimus and Morgan, 2004).

Preparation of Pure ER Fractions
Supernatants from the 600 × g centrifugation step were prepared as described in the Extended Experimental Procedures. Next, the "Sigma-Endoplasmic Reticulum Isolation Kit" was used according to the manufacturer's protocol.

ATP Content Determination
ATP concentration was determined using the "CellTiter Glo" assay (Promega USA) according to the manufacturer's instructions. The results were normalized to protein concentration.

SUPPLEMENTAL INFORMATION

Supplemental Information includes Extended Experimental Procedures and seven figures and can be found with this article online at http://dx.doi.org/10.1016/j.celrep.2012.10.009.

LICENSING INFORMATION

REFERENCES

Arismendi-Morillo, G. (2011). Electron microscopy morphology of the mitochondrial network in gliomas and their vascular microenvironment. Biochim. Biophys. Acta *1807*, 602–608.

Batandier, C., Guigas, B., Detaille, D., El-Mir, M.Y., Fontaine, E., Rigoulet, M., and Leverve, X.M. (2006). The ROS production induced by a reverse-electron flux at respiratory-chain complex 1 is hampered by metformin. J. Bioenerg. Biomembr. *38*, 33–42.

Baud, V., and Karin, M. (2009). Is NF-κB a good target for cancer therapy? Hopes and pitfalls. Nat. Rev. Drug Discov. *8*, 33–40.

Bell, E.L., Klimova, T.A., Eisenbart, J., Moraes, C.T., Murphy, M.P., Budinger, G.R., and Chandel, N.S. (2007). The Qo site of the mitochondrial complex III is required for the transduction of hypoxic signaling via reactive oxygen species production. J. Cell Biol. *177*, 1029–1036.

Bental, M., and Deutsch, C. (1993). Metabolic changes in activated T cells: an NMR study of human peripheral blood lymphocytes. Magn. Reson. Med. *29*, 317–326.

Chowdhury, S.K., Gemin, A., and Singh, G. (2005). High activity of mitochondrial glycerophosphate dehydrogenase and glycerophosphate-dependent ROS production in prostate cancer cell lines. Biochem. Biophys. Res. Commun. *333*, 1139–1145.

Collison, L.W., Murphy, E.J., and Jolly, C.A. (2008). Glycerol-3-phosphate acyltransferase-1 regulates murine T-lymphocyte proliferation and cytokine production. Am. J. Physiol. Cell Physiol. *295*, C1543–C1549.

Cottingham, I.R., and Ragan, C.I. (1980). The reconstitution of L-3-glycerophosphate-cytochrome *c* oxidoreductase from L-3-glycerophosphate dehydrogenase, ubiquinone-10 and ubiquinol-cytochrome *c* oxidoreductase. Biochem. J. *192*, 19–31.

Devadas, S., Zaritskaya, L., Rhee, S.G., Oberley, L., and Williams, M.S. (2002). Discrete generation of superoxide and hydrogen peroxide by T cell receptor

stimulation: selective regulation of mitogen-activated protein kinase activation and fas ligand expression. J. Exp. Med. *195*, 59–70.

Doherty, M., Boot-Handford, R.P., Grant, M.E., and Canfield, A.E. (1998). Identification of genes expressed during the osteogenic differentiation of vascular pericytes in vitro. Biochem. Soc. Trans. *26*, S4.

Dröge, W. (2002). Free radicals in the physiological control of cell function. Physiol. Rev. *82*, 47–95.

Dröse, S., and Brandt, U. (2012). Molecular mechanisms of superoxide production by the mitochondrial respiratory chain. Adv. Exp. Med. Biol. *748*, 145–169.

Dröse, S., Bleier, L., and Brandt, U. (2011). A common mechanism links differently acting complex II inhibitors to cardioprotection: modulation of mitochondrial reactive oxygen species production. Mol. Pharmacol. *79*, 814–822.

Feske, S. (2007). Calcium signalling in lymphocyte activation and disease. Nat. Rev. Immunol. *7*, 690–702.

Gao, X., Wang, H., Yang, J.J., Liu, X., and Liu, Z.R. (2012). Pyruvate kinase M2 regulates gene transcription by acting as a protein kinase. Mol. Cell *45*, 598–609.

Gülow, K., Kaminski, M., Darvas, K., Süss, D., Li-Weber, M., and Krammer, P.H. (2005). HIV-1 trans-activator of transcription substitutes for oxidative signaling in activation-induced T cell death. J. Immunol. *174*, 5249–5260.

Guppy, M., Greiner, E., and Brand, K. (1993). The role of the Crabtree effect and an endogenous fuel in the energy metabolism of resting and proliferating thymocytes. Eur. J. Biochem. *212*, 95–99.

Hruz, T., Laule, O., Szabo, G., Wessendorp, F., Bleuler, S., Oertle, L., Widmayer, P., Gruissem, W., and Zimmermann, P. (2008). Genevestigator v3: a reference expression database for the meta-analysis of transcriptomes. Adv. Bioinforma. *2008*, 420747.

Idahl, L.A., and Lembert, N. (1995). Glycerol 3-phosphate-induced ATP production in intact mitochondria from pancreatic B-cells. Biochem. J. *312*, 287–292.

Jackson, S.H., Devadas, S., Kwon, J., Pinto, L.A., and Williams, M.S. (2004). T cells express a phagocyte-type NADPH oxidase that is activated after T cell receptor stimulation. Nat. Immunol. *5*, 818–827.

Jacobs, S.R., Herman, C.E., Maciver, N.J., Wofford, J.A., Wieman, H.L., Hammen, J.J., and Rathmell, J.C. (2008). Glucose uptake is limiting in T cell activation and requires CD28-mediated Akt-dependent and independent pathways. J. Immunol. *180*, 4476–4486.

Jones, R.G., Bui, T., White, C., Madesh, M., Krawczyk, C.M., Lindsten, T., Hawkins, B.J., Kubek, S., Frauwirth, K.A., Wang, Y.L., et al. (2007). The proapoptotic factors Bax and Bak regulate T Cell proliferation through control of endoplasmic reticulum Ca²⁺ homeostasis. Immunity *27*, 268–280.

Kamiński, M., Kiessling, M., Süss, D., Krammer, P.H., and Gülow, K. (2007). Novel role for mitochondria: protein kinase Cθ-dependent oxidative signaling organelles in activation-induced T-cell death. Mol. Cell. Biol. *27*, 3625–3639.

Kamiński, M.M., Sauer, S.W., Klemke, C.D., Süss, D., Okun, J.G., Krammer, P.H., and Gülow, K. (2010). Mitochondrial reactive oxygen species control T cell activation by regulating IL-2 and IL-4 expression: mechanism of ciprofloxacin-mediated immunosuppression. J. Immunol. *184*, 4827–4841.

Kamiński, M.M., Röth, D., Sass, S., Sauer, S.W., Krammer, P.H., and Gülow, K. (2012). Manganese superoxide dismutase: a regulator of T cell activation-induced oxidative signaling and cell death. Biochim. Biophys. Acta *1823*, 1041–1052.

Krawczyk, C.M., Holowka, T., Sun, J., Blagih, J., Amiel, E., DeBerardinis, R.J., Cross, J.R., Jung, E., Thompson, C.B., Jones, R.G., and Pearce, E.J. (2010). Toll-like receptor-induced changes in glycolytic metabolism regulate dendritic cell activation. Blood *115*, 4742–4749.

Krivanek, J., and Novakova, L. (1991). ATP-citrate lyase is another enzyme the histidine phosphorylation of which is inhibited by vanadate. FEBS Lett. *282*, 32–34.

Kwon, J., Shatynski, K.E., Chen, H., Morand, S., de Deken, X., Miot, F., Leto, T.L., and Williams, M.S. (2010). The nonphagocytic NADPH oxidase Duox1

mediates a positive feedback loop during T cell receptor signaling. Sci. Signal. *3*, ra59.

Lambert, A.J., and Brand, M.D. (2009). Reactive oxygen species production by mitochondria. Methods Mol. Biol. *554*, 165–181.

Los, M., Schenk, H., Hexel, K., Baeuerle, P.A., Dröge, W., and Schulze-Osthoff, K. (1995). IL-2 gene expression and NF-κB activation through CD28 requires reactive oxygen production by 5-lipoxygenase. EMBO J. *14*, 3731–3740.

Mannella, C.A. (2006). Structure and dynamics of the mitochondrial inner membrane cristae. Biochim. Biophys. Acta *1763*, 542–548.

Miccheli, A., Tomassini, A., Puccetti, C., Valerio, M., Peluso, G., Tuccillo, F., Calvani, M., Manetti, C., and Conti, F. (2006). Metabolic profiling by 13C-NMR spectroscopy: [1,2-13C2]glucose reveals a heterogeneous metabolism in human leukemia T cells. Biochimie *88*, 437–448.

Miwa, S., St-Pierre, J., Partridge, L., and Brand, M.D. (2003). Superoxide and hydrogen peroxide production by Drosophila mitochondria. Free Radic. Biol. Med. *35*, 938–948.

Netzker, R., Greiner, E., Eigenbrodt, E., Noguchi, T., Tanaka, T., and Brand, K. (1992). Cell cycle-associated expression of M2-type isozyme of pyruvate kinase in proliferating rat thymocytes. J. Biol. Chem. *267*, 6421–6424.

Nishikawa, T., Edelstein, D., Du, X.L., Yamagishi, S., Matsumura, T., Kaneda, Y., Yorek, M.A., Beebe, D., Oates, P.J., Hammes, H.P., et al. (2000). Normalizing mitochondrial superoxide production blocks three pathways of hyperglycaemic damage. Nature *404*, 787–790.

Qin, J., Chai, G., Brewer, J.M., Lovelace, L.L., and Lebioda, L. (2006). Fluoride inhibition of enolase: crystal structure and thermodynamics. Biochemistry *45*, 793–800.

Richter, S., Richter, J.P., Mehta, S.Y., Gribble, A.M., Sutherland-Smith, A.J., Stowell, K.M., Print, C.G., Ronimus, R.S., and Wilson, W.R. (2012). Expression and role in glycolysis of human ADP-dependent glucokinase. Mol. Cell. Biochem. *364*, 131–145.

Ronimus, R.S., and Morgan, H.W. (2004). Cloning and biochemical characterization of a novel mouse ADP-dependent glucokinase. Biochem. Biophys. Res. Commun. *315*, 652–658.

Rutter, G.A., Pralong, W.F., and Wollheim, C.B. (1992). Regulation of mitochondrial glycerol-phosphate dehydrogenase by Ca²⁺ within electropermeabilized insulin-secreting cells (INS-1). Biochim. Biophys. Acta *1175*, 107–113.

Stentz, F.B., and Kitabchi, A.E. (2005). Hyperglycemia-induced activation of human T-lymphocytes with de novo emergence of insulin receptors and generation of reactive oxygen species. Biochem. Biophys. Res. Commun. *335*, 491–495.

Tretter, L., Takacs, K., Hegedus, V., and Adam-Vizi, V. (2007). Characteristics of α-glycerophosphate-evoked H2O2 generation in brain mitochondria. J. Neurochem. *100*, 650–663.

Tsuge, H., Sakuraba, H., Kobe, T., Kujime, A., Katunuma, N., and Ohshima, T. (2002). Crystal structure of the ADP-dependent glucokinase from *Pyrococcus horikoshii* at 2.0-Å resolution: a large conformational change in ADP-dependent glucokinase. Protein Sci. *11*, 2456–2463.

Tu, K.Y., Ju, H.S., Pettit, F., Shive, W., Topek, N.H., Matthews, R., and Matthews, K. (1995). Glycerol-3-phosphate dehydrogenase activity in human lymphocytes: effects of insulin, obesity and weight loss. Biochem. Biophys. Res. Commun. *207*, 183–190.

Vander Heiden, M.G., Cantley, L.C., and Thompson, C.B. (2009). Understanding the Warburg effect: the metabolic requirements of cell proliferation. Science *324*, 1029–1033.

Vander Heiden, M.G., Locasale, J.W., Swanson, K.D., Sharfi, H., Heffron, G.J., Amador-Noguez, D., Christofk, H.R., Wagner, G., Rabinowitz, J.D., Asara, J.M., and Cantley, L.C. (2010). Evidence for an alternative glycolytic pathway in rapidly proliferating cells. Science *329*, 1492–1499.

Wang, T., Marquardt, C., and Foker, J. (1976). Aerobic glycolysis during lymphocyte proliferation. Nature *261*, 702–705.

Warburg, O. (1956). On respiratory impairment in cancer cells. Science *124*, 269–270.

Wellen, K.E., and Thompson, C.B. (2010). Cellular metabolic stress: considering how cells respond to nutrient excess. Mol. Cell *40*, 323–332.

Wick, A.N., Drury, D.R., Nakada, H.I., and Wolfe, J.B. (1957). Localization of the primary metabolic block produced by 2-deoxyglucose. J. Biol. Chem. *224*, 963–969.

Wilson, J.E. (2003). Isozymes of mammalian hexokinase: structure, subcellular localization and metabolic function. J. Exp. Biol. *206*, 2049–2057.

Wu, C., Orozco, C., Boyer, J., Leglise, M., Goodale, J., Batalov, S., Hodge, C.L., Haase, J., Janes, J., Huss, J.W., 3rd, and Su, A.I. (2009). BioGPS: an extensible and customizable portal for querying and organizing gene annotation resources. Genome Biol. *10*, R130.

Yi, J.S., Holbrook, B.C., Michalek, R.D., Laniewski, N.G., and Grayson, J.M. (2006). Electron transport complex I is required for CD8+ T cell function. J. Immunol. *177*, 852–862.